

Seasonal Evolution of Subtropical Anticyclones in the Climate System Model FGOALS-s2

LIU Yimin^{*1} (刘屹岷), HU Jun¹ (胡俊), HE Bian^{2,1} (何编), BAO Qing¹ (包庆), DUAN Anmin¹ (段安民), and WU Guoxiong¹ (吴国雄)

¹*State Key Laboratory of Numerical Modeling for Atmospheric Sciences and Geophysical Fluid Dynamics,*

Institute of Atmospheric Physics, Chinese Academy of Sciences, Beijing 100029

²*Nanjing University of Information Science and Technology, Nanjing 210044*

(Received 15 July 2012; revised 15 November, 2012)

ABSTRACT

The simulation characteristics of the seasonal evolution of subtropical anticyclones in the Northern Hemisphere are documented for the Flexible Global Ocean-Atmosphere-Land System model, Spectral Version 2 (FGOALS-s2), developed at the State Key Laboratory of Numerical Modeling for Atmospheric Sciences and Geophysical Fluid Dynamics, the Institute of Atmospheric Physics. An understanding of the seasonal evolution of the subtropical anticyclones is also addressed. Compared with the global analysis established by the European Centre for Medium-Range Forecasts, the ERA-40 global reanalysis data, the general features of subtropical anticyclones and their evolution are simulated well in both winter and summer, while in spring a pronounced bias in the generation of the South Asia Anticyclone (SAA) exists. Its main deviation in geopotential height from the reanalysis is consistent with the bias of temperature in the troposphere. It is found that condensation heating (CO) plays a dominant role in the seasonal development of the SAA and the subtropical anticyclone over the western Pacific (SAWP) in the middle troposphere. The CO biases in the model account for the biases in the establishment of the SAA in spring and the weaker strength of the SAA and the SAWP from spring to summer. CO is persistently overestimated in the central-east tropical Pacific from winter to summer, while it is underestimated over the area from the South China Sea to the western Pacific from spring to summer. Such biases generate an illusive anticyclonic gyre in the upper troposphere above the middle Pacific and delay the generation of the SAA over South Asia in April. In mid-summer, the simulated SAA is located farther north than in the ERA-40 data owing to excessively strong surface sensible heating (SE) to the north of the Tibetan Plateau. Whereas, the two surface subtropical anticyclones in the eastern oceans during spring to summer are controlled mainly by the surface SE over the two continents in the Northern Hemisphere, which are simulated reasonably well, albeit with their centers shifted westwards owing to the weaker longwave radiation cooling in the simulation associated with much weaker local stratiform cloud. Further improvements in the related parameterization of physical processes are therefore identified.

Key words: subtropical anticyclone simulation, seasonal evolution, components of diabatic heating, climate system model FGOALS-s2

Citation: Liu, Y. M., J. Hu, B. He, Q. Bao, A. M. Duan, and G. X. Wu, 2013: Seasonal evolution of subtropical anticyclones in the climate system model FGOALS-s2. *Adv. Atmos. Sci.*, **30**(3), 593–606, doi: 10.1007/s00376-012-2154-0.

1. Introduction

A subtropical anticyclone (SA) connects westerlies to its north and easterlies to its south. The seasonal development of the South Asian Anticyclone (SAA)

in the upper troposphere and Subtropical Anticyclone over the Western Pacific (SAWP) in the middle troposphere are closely related to the seasonal variation of moisture transport and East Asian monsoon rainfall (Wu et al., 2002), making SA simulation an important

* Corresponding author: LIU Yimin, lym@lasg.iap.ac.cn

part of any climate model.

In winter, westerlies dominate in the mid-latitudes and subtropics in the free troposphere and mountain forcing plays an important role in the formation of the circulation patterns in these areas (Charney and Eliassen, 1949; Yeh, 1950; Rodwell and Hoskins, 2001). Conversely, in subtropical summers, the westerlies are weak and thermal forcing becomes more important in influencing the circulation pattern (Hoskins, 1987). The diabatic heating has three components: radiative heating, condensation heating, and the sensible heating (SE) in the boundary layer (Newell et al., 1970). Wu et al. (2003) and Liu et al. (2004b, 2007) investigated the relative effectiveness of different components of diabatic heating and their synthetic effects on the formation of summertime subtropical anticyclones (Wu et al., 2009). They showed that in subtropical summers over each continent and its adjacent oceans from west to east, longwave radiative cooling (LO), land surface sensible heating (SE), condensation heating (CO), and double-dominant heating (D; includes CO and LO) compose such a LOSECOD heating quadruplet. A specific zonal asymmetric circulation pattern is then formed in response to the quadruplet heating. However, what dominates SA development during the seasonal transition from winter to summer remains unknown.

The Flexible Global Ocean-Atmosphere-Land System model, Spectral Version 2 (FGOALS-s2) is a climate model consisting of atmosphere, land, ocean, and sea ice components linked through a coupler that exchanges state information and fluxes among the components. FGOALS is developed at the State Key Laboratory of Numerical Modeling for Atmospheric Sciences and Geophysical Fluid Dynamics, the Institute of Atmospheric Physics (LASG/IAP). FGOALS and its atmosphere component SAMIL (Spectral Atmospheric General Circulation Model of the LASG/IAP) have been used to study the East Asian Summer Monsoon (Wang et al., 2007, 2012), the formation of SAs in summertime (Liu et al., 2001, 2004b), and the impacts of the Tibetan Plateau(TP) (Wu et al., 2007; Duan et al., 2008; Yu et al., 2011). An overview paper by Bao et al. (2013) describes some of the most important developments and improvements in the model components of the most recent version FGOALS.

In the study reported in the present paper, simulation of the seasonal evolution of an SA from winter to summer was examined in detail. Rather than making comparisons with earlier versions of the model, we focused on comparing with reanalysis data and documenting the deviation and associated physical processes to further understand the mechanism underlying SA seasonal development, with the ultimate aim

to help improve the next generation of climate model.

The remainder of the paper is organized as follows. In section 2 we describe the data, FGOALS-s2, and the experimental design used for the study. Section 3 presents the SA simulation results, comparing them to observations in reanalysis data. Section 4 focuses on the mechanisms responsible for the main biases of the model in simulating the seasonal evolution of the SA. And finally, a discussion and conclusion are presented in section 5.

2. Model and data

FGOALS-s2 contains a spectral atmospheric model truncated at R42 [approximately 1.66° (lat) $\times 2.81^\circ$ (lon)], namely SAMIL2, and is coupled to land and sea ice components as well as a 1° -resolution (with 0.5° meridional resolution in the tropics) ocean model (LICOM) (Liu et al., 2004a, 2012). Grid points in the atmospheric model have 26 levels in the vertical direction. The ocean component is the second version of LICOM (LICOM2) with 30 levels in the vertical direction, which is also developed at the LASG. The land and sea ice components are the Community Land Model version 3 (CLM3) and Community Sea-Ice Model Version 4 (CSIM4) respectively, from the third version of the Community Climate System Model (CCSM3) (Collins et al., 2006). No flux adjustments are used. Experimental results employed for this study include the three ensembles of the 20th century simulations with a combination of anthropogenic and natural forcing, which is a branch from a multi-century pre-industrial control run from 1850–2005 (Bao et al., 2012).

For validating the simulation of SA seasonal variation, two atmospheric reanalysis datasets were used: the global analysis established by the European Centre for Medium-Range Forecasts (ECMWF) (ERA-40; Uppala et al., 2005) and the Japanese reanalysis project (JRA-25; Onogi et al., 2007). The resolution of the total column diabatic heating of ERA-40 is $1.125^\circ \times 1.125^\circ$ and its circulation is $2.5^\circ \times 2.5^\circ$ for the period 1958–2002. The horizontal resolution of JRA-25's geopotential height (GPH) is $1.25^\circ \times 1.25^\circ$ for the period 1979–2002.

3. Seasonal evolution of the SA

In boreal summer, the atmospheric circulation over Asia is characterized by the existence of two persistent SA systems. One is the pronounced SAA in the upper troposphere, just above the region to the north of the Bay of Bengal (BOB) (Fig. 1); and the other, the SAWP in the middle troposphere. In winter, mean-

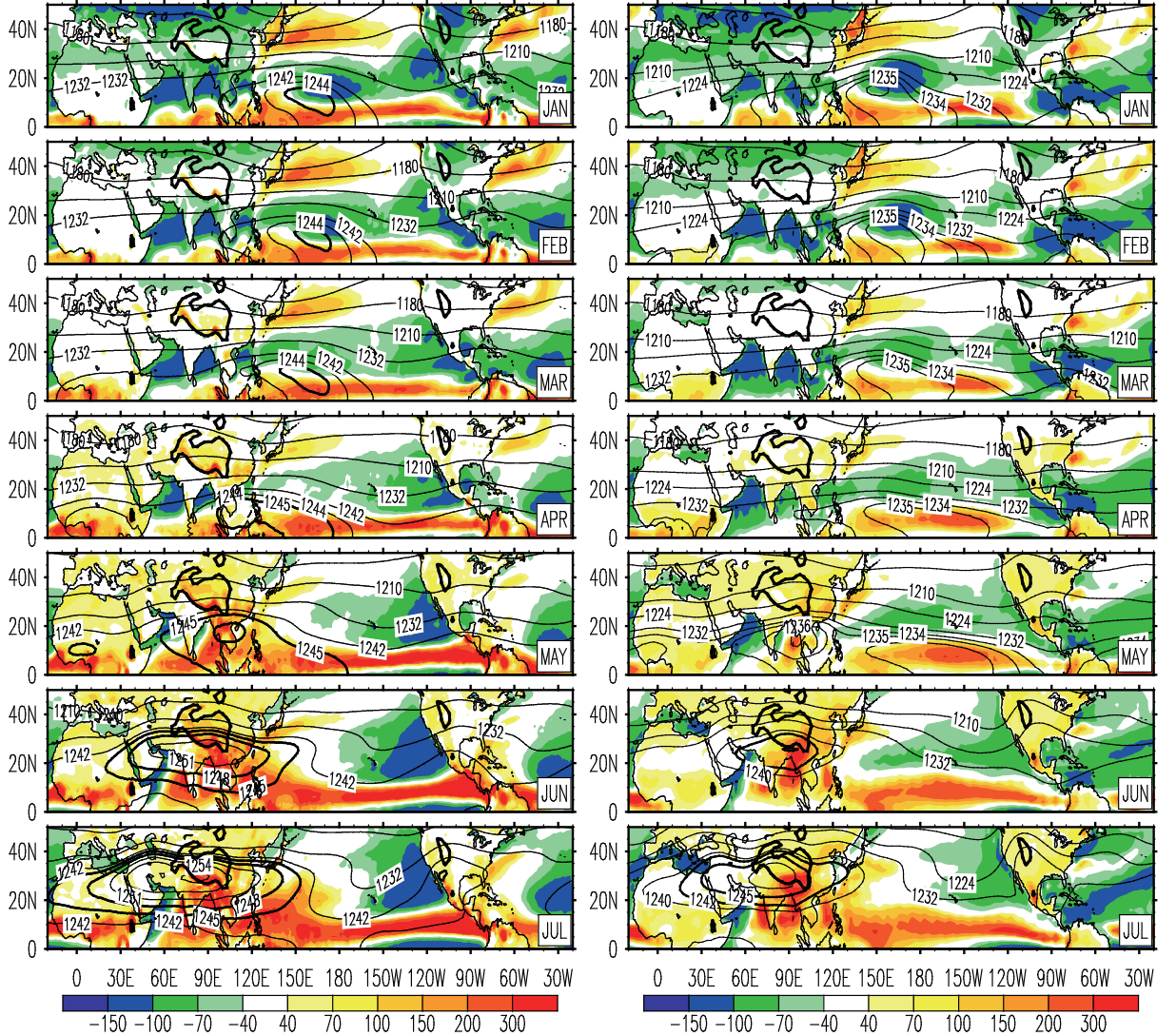


Fig. 1. Monthly mean GPH (units: dgpm) at 200 hPa and total diabatic heating (units: W m^{-2}) from ERA-40 (left) and FGOALS-s2 (right). January to July is represented from top to bottom. The thick contours show the GPH of 1245 and 1248 dgpm, respectively.

while, there exist only long waves over the Eurasian continent, and the closed anticyclone circulation is located over the western Pacific in the mid-upper troposphere. The SAWP (Fig. 4) as well as the SA near the surface exist in all seasons and their seasonal evolutions exhibit movements in location and variations in strength. However, unlike the SAWP, the SAA does not exist in winter. As indicated by Liu et al. (2009) and the following examination, the SAA is established over the Indochina Peninsula during spring.

3.1 SAA

Figure 1 shows climatological seasonal evolution of GPH and total diabatic heating from winter to summer, i.e. from January to July in both ERA-40 and

FGOALS-s2. The ERA-40 reanalysis shows that the East Asian Trough (EAT) is situated over the mid and high latitudes of the Asian coast and an enclosed anticyclone is stably located over the tropical western Pacific during the winter and early spring (March). The anticyclone is located between a strong cooling in the subtropical western Pacific and a warming of the ITCZ in the south. In April, the anticyclone is weakened, while the diabatic heating is enhanced over the Asian continent, especially over South China and the Indochina Peninsula. Thus, high pressure develops over the South China Sea (SCS) and can be named as the SAA. In May, the SAA center is over the Indochina Peninsula. It develops further in June and jumps to the south of the TP and South Asia. The

SAA summer pattern from ERA-40 looks similar to that from the National Centers for Environmental Prediction (NCEP) reanalysis data (Li, 2001; Wu et al., 2002). During July and August (data not shown) the SAA is even stronger above the TP, in fact achieving its maximum strength. Correspondingly, to the east of the SAA the tropical upper-tropospheric trough (TUTT) is strongest during July and August.

FGOALS-s2 is able to simulate the characteristics of the winter EAT and the enclosed anticyclone over the western Pacific very well, except the magnitude of the GPH is weaker (right panels in Fig. 1) than in ERA-40 (left panels of Fig. 1) and the geopotential high center over the western Pacific is shifted about 5° northward. The location deviation is acceptable, as we can identify a 5° zonal difference in the location between ERA-40 and JRA-25 during January–March (Fig. 2). The magnitude of the GPH value is still smaller during later spring and summer, indicating that the strength of the modeled SAA is weaker than ERA-40 during and after it is generated.

The largest deviation of the GPH appears in April and May. Although a high ridge extends westward to the southern SCS, the GPH is strengthened more near to the dateline (right panels of Fig. 1) rather than over the SCS as in ERA-40 (left panels of Fig. 1), corresponding to the overestimated diabatic heating near the date line. We will see later that the total heating deviation is mainly from condensation heating (Figs. 1 and 4). Thus, the simulated SAA is very weak in April. The strength of the simulated SAA becomes better in May, but a high level of deviation still exists over the dateline compared to ERA-40. The GPH remains higher in the central equatorial Pacific, such that the FGOALS-s2 TUTT is weaker than that in the observation in summer. Comparing the simulated total diabatic heating (shading in right panels of Fig. 1)

to ERA-40 (left panels of Fig. 1), the total heating associated with the LO over the Eastern Pacific is underestimated by $10\text{--}50 \text{ W m}^{-2}$, which induces anticyclonic deviation and also contributes to the weakening of the TUTT in the upper troposphere and the westward shifting of the subtropical anticyclone center near the surface, as shown in Fig. 6.

The SAA in FGOALS-s2 shifts northwestward during June and its center is located towards the southwestern TP, reflecting well the ERA-40 observation, albeit showing less strength. In July, FGOALS-s2 simulates the SAA very well. However, by comparing the right and left panels in Fig. 1 in detail, it can be seen that the simulated enclosed SAA expands farther northeastwards than in ERA-40 in July.

To clearly show the seasonal development of the SAA's location, Fig. 2 presents the evolution of the location of the SAA center from ERA-40 and FGOALS-s2, as well as from JRA-25 reanalysis, by using data with a common period of coverage (1979–2002). For convenience, here we temporarily use "SAA" to indicate the anticyclone over the western Pacific before the SAA is established in April. It shows that from January to March the anticyclone center (maximum GPH) is around $150^{\circ}\text{--}160^{\circ}\text{E}$, and the differences between ERA-40 and JRA-25 are less than 10° , except in April. In April, the SAA center is at 110°E in ERA-40, but 150°E in JRA-25 – a 40° eastward shift. The simulated maximum GPH is located even farther eastwards, at around 165°W . In May, the center of the SAA in the two reanalyses and the simulation is above the Indochina Peninsula. The SAA moves farther towards the TP and stabilizes at $(30^{\circ}\text{N}, 80^{\circ}\text{E})$ during mid-summer (July and August). Corresponding to the northeastward tilt of the modeled SAA (right panels of Fig. 1), the location of the simulated SAA center is shifted to the northeast of its counterpart in the ERA-

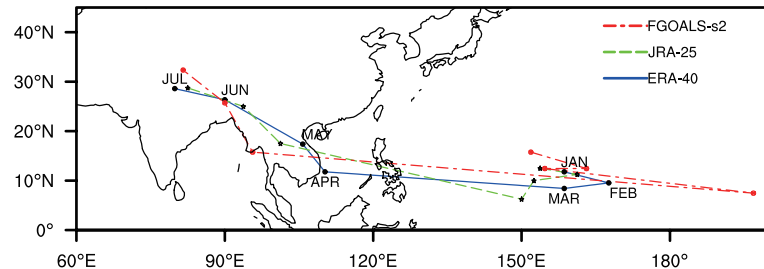


Fig. 2. Seasonal evolution from January to July of the center of the tropical GPH over the western Pacific/SAA produced from ERA-40 (blue), JRA-25 (green) and FGOALS-s2 (red). The center location is the position of the maximum GPH over different months, i.e. $(0^{\circ}\text{--}40^{\circ}\text{N}, 110^{\circ}\text{E}\text{--}150^{\circ}\text{W})$ for December–April; $(0^{\circ}\text{--}40^{\circ}\text{N}, 70^{\circ}\text{--}150^{\circ}\text{E})$ for May, October and November; and $(0^{\circ}\text{--}40^{\circ}\text{N}, 30^{\circ}\text{--}140^{\circ}\text{E})$ for June–September.

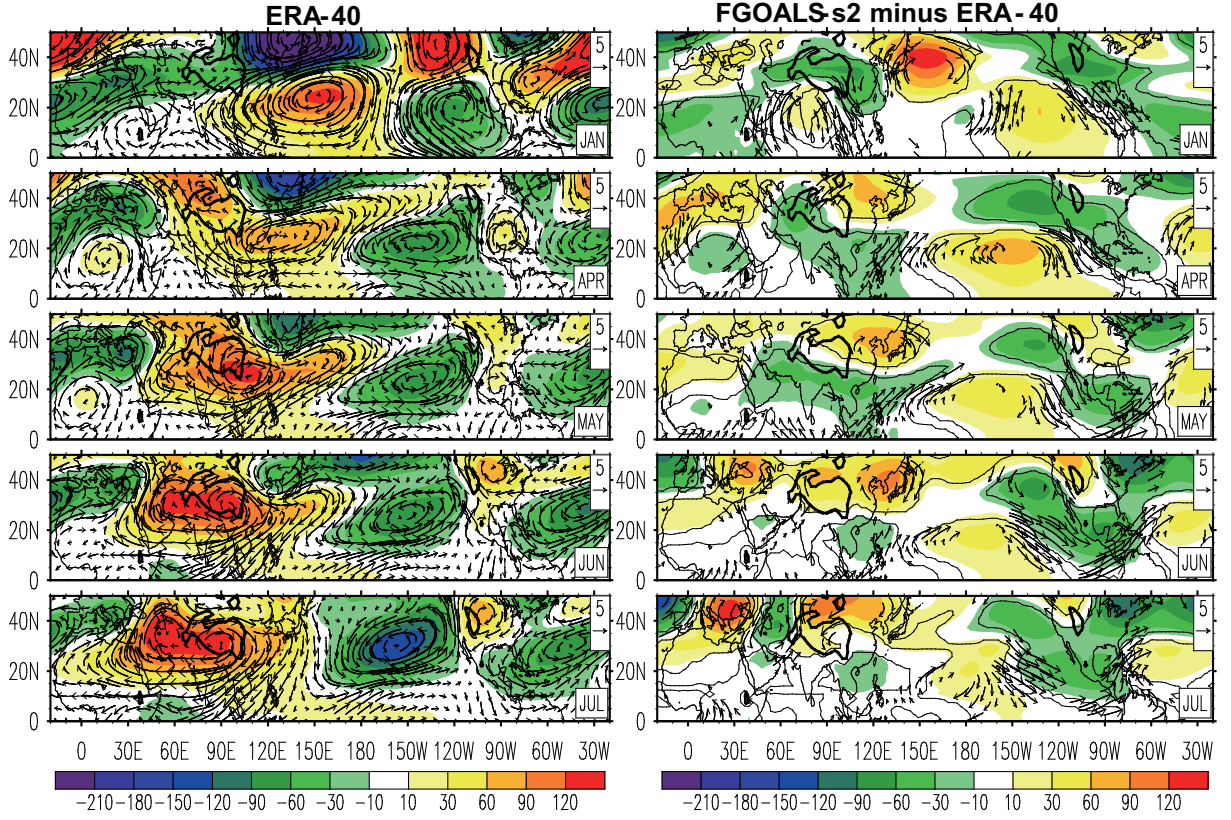


Fig. 3. Mean zonal deviation of GPH (shaded; units: gpm) and wind (vector; units: m s^{-1}) at 200 hPa from ERA-40 (left) and their differences between FGOALS-s2 and ERA-40 (right). January and April to July are represented from top to bottom. Black lines and wind vectors on the right panels mean that differences are statistically significant at the 99% level according to the Student's *t*-test.

40 reanalysis.

Zonal deviation of GPH is usually used to present the stationary wave, and the pattern for 200 hPa in ERA-40 is given in the left panels of Fig. 3. To quantitatively show the biases of the FGOALS-s2 simulation to ERA-40, the zonal deviation differences of GPH between the two datasets is given in the right panels of Fig. 3. Since the pattern is stable in winter and early spring (Fig. 1), February and March are omitted in Fig. 3.

There are distinct differences in the stationary wave pattern between winter and summer in the observation (left panels of Fig. 3). An anticyclone is located over the western tropical Pacific in winter and over the Eurasian continent in summer. A cyclone associated with the TUTT is located to the east of the anticyclone and always over the eastern Pacific, though moving northwestward in summer. In April, an anticyclone with higher GPH is established over the area from the TP to South Asia and the western Pacific, and the TUTT extends westwards to the west of the date line. In June and July the SAA is stable, cov-

ering an area from continental subtropical Eurasia to the western Pacific. Compared to the GPH pattern in which the SAA center is located to the south of 30°N in July (left panels of Fig. 1), the anticyclone center produced by the zonal derivation wind and GPH is located farther northwards (left panels of Fig. 3).

In winter, the obvious bias is from India to the mid-high latitudes over the coast Asia (right panels of Fig. 3), presenting a Rossby wave emanating from India and propagating to the east of Japan via the TP and east China. The positive GPH difference and anticyclone to the east of Japan indicate that the simulated EAT is weaker. There is always an anticyclone bias over the tropical eastern Pacific. It shifts westwards from winter to summer with the maximum in April and the minimum in July. In April, above the SCS where the observed SAA center is located, the GPH is underestimated such that the SAA is much weaker in the simulation than the observation during its generation stage. In summer (June and July), the negative bias exists over South Asia and the positive to the north of the TP, indicating an underestimation of

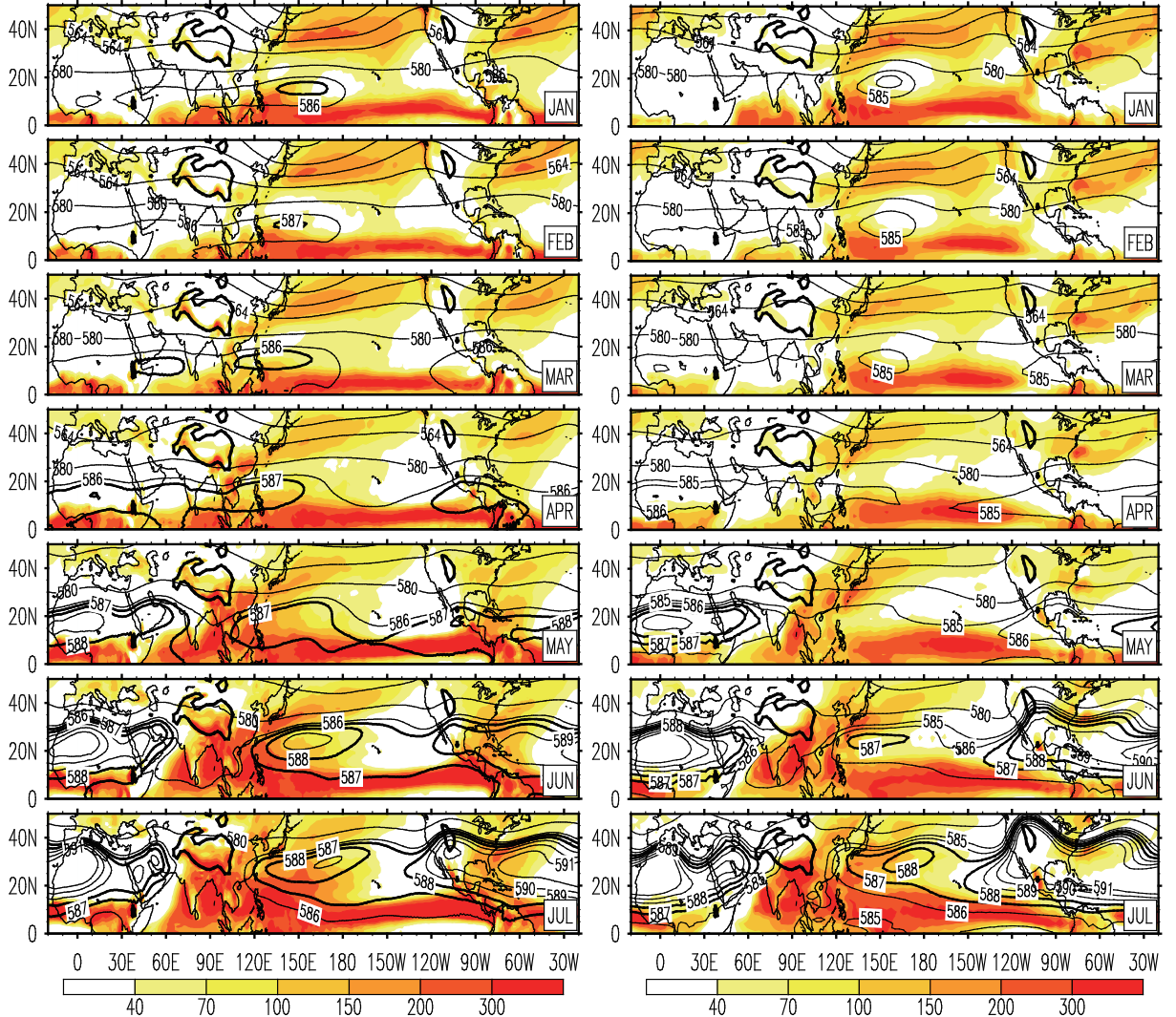


Fig. 4. Mean GPH (units: dgpm) at 500 hPa and CO (units: W m^{-2}) from ERA-40 (left) and FGOALS-s2 (right). January to July is represented from top to bottom. The thick contours show the GPH of 587 and 588 dgpm, respectively.

the SAA strength in the simulation, but an overestimation of the GPH to the north of the SAA. The persistent anticyclone bias over the tropical central/eastern Pacific in summer implies an underestimated TUTT in the simulation.

3.2 SAWP in the middle troposphere

For validating the SAWP simulation we use the GPH at 500 hPa, and Fig. 4 shows the ERA-40 observation (left panels) and FGOALS-s2 simulation (right panels). Both sets of data demonstrate that the main body of the SAWP is located over the western Pacific in all seasons. The main characteristics of the seasonal variation of the SAWP are the northward movement and strengthening from winter to summer,

especially from spring to summer. Compared to its previous version (data not shown; refer to Wu et al., 2003), FGOALS-s2 has improved its simulation of the SAWP both in terms of pattern and intensity. The belt pattern of subtropical high-pressure in winter, an inserted trough over the middle Pacific in spring (March and April) along the subtropics, and the enhanced and northwestward shift of the anticyclone over the western Pacific from spring to summer in the simulation, also emulate those features in the ERA-40 very well (Fig. 4).

However, some biases still exist. The differences in the zonal deviation between FGOALS-s2 and ERA-40 at 500 hPa (left panels of Fig. 5) and 200 hPa (right panels of Fig. 3) show that in the mid-high lati-

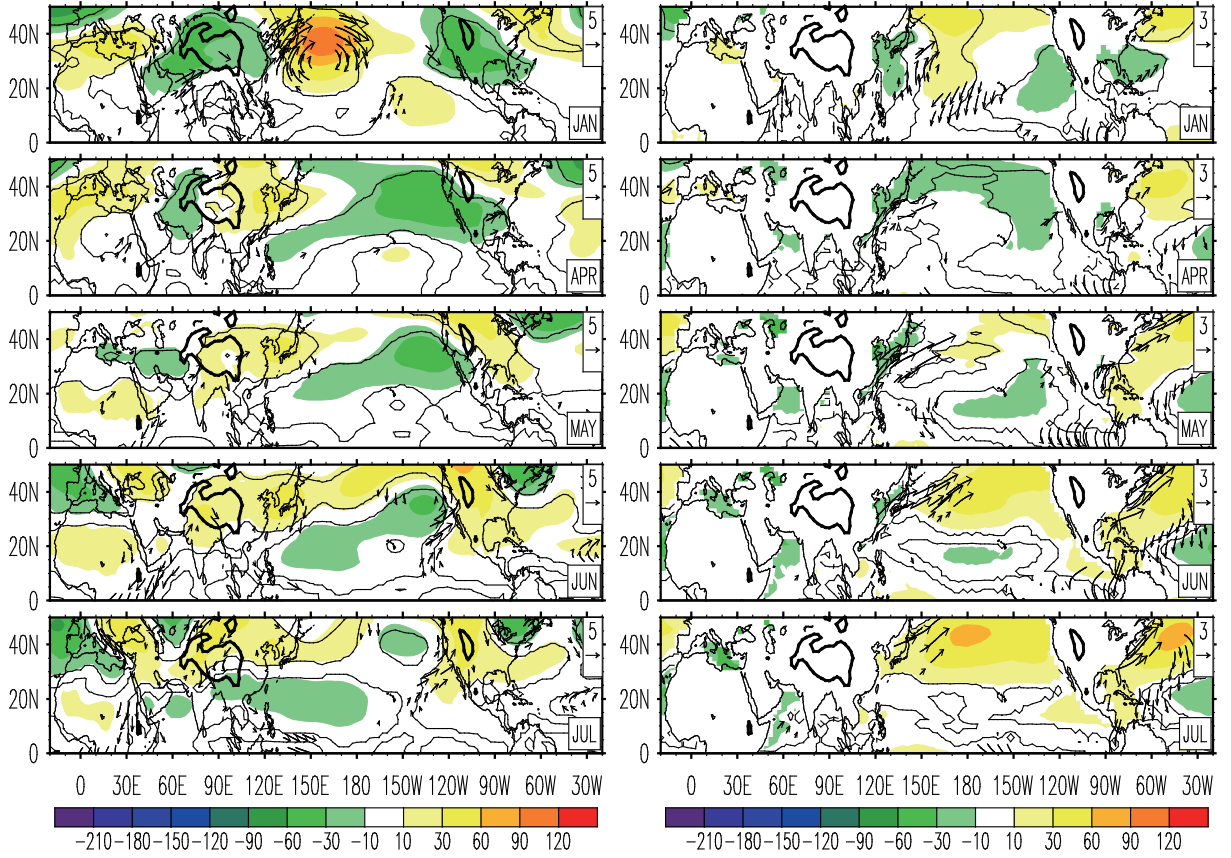


Fig. 5. Differences of zonal deviation of GPH (shaded; units: gpm) and wind (vector; units m s^{-1}) between FGOALS-s2 and ERA-40 at 500 hPa (left) and 1000 hPa (right). January and April to July are represented from top to bottom. Black curves and wind vectors denote the differences are statistically significant at the 99% level according to the Student's *t*-test.

tudes the bias presents an equivalent barotropic structure in wintertime. Moreover, in winter the SAWP in FGOALS-s2 is located about 4° north of its ERA-40 counterpart (Fig. 4). Such bias can also be detected in the SAA's simulation at 200 hPa (Fig. 1). But these biases are weaker in their zonal deviation pattern (upper-left panels of Fig. 5), which implies the zonal pressure gradient is well simulated. The negative biases during spring to summer shown in the left panels of Fig. 5 indicate that the strength of the SAWP is underestimated. The GPH in Fig. 4 also shows that the SAWP is 10–20gpm less in the simulation than in ERA-40 over the western Pacific. From May, a trough is generated over the BOB and obtains its maximum in mid-summer (left panels of Fig. 4). This trough in FGOALS-s2 is also weaker than in ERA-40, corresponding to the weaker SAWP (left panels of Fig. 5).

3.3 SA over the eastern Pacific and Atlantic

Besides the SAA and the SAWP, the SA over the eastern Pacific (SAEP) and eastern Atlantic (SAEA)

dominate the circulation near the surface. The SAEP and SAEA are much weaker in winter, but strongest in summer in ERA-40 (left panels of Fig. 6), again similar to those from NCEP reanalysis data (Liu et al., 1999; Li, 2001). From winter to summer, the main body of the SAEP and the SAEA extends westwards. FGOALS-s2 captures such a seasonal development very well (right panels of Fig. 6).

There are two main biases in the surface SA simulation. One is that the simulation of the zonal pressure is too symmetric in winter over the subtropical Pacific. In winter, the Aleutian Low is located at middle and high latitudes over the northern Pacific. It extends southwestwards and low pressure dominates the western Pacific, leading to the SAEP being weak and located only over a small domain in the eastern Pacific over the subtropics during winter and early spring (left panels of Fig. 6). However, FGOALS-s2 generates a rather zonal symmetric high over the subtropical ocean during this period (right panels of Fig. 6). The other bias is the strength and location of the two surface an-

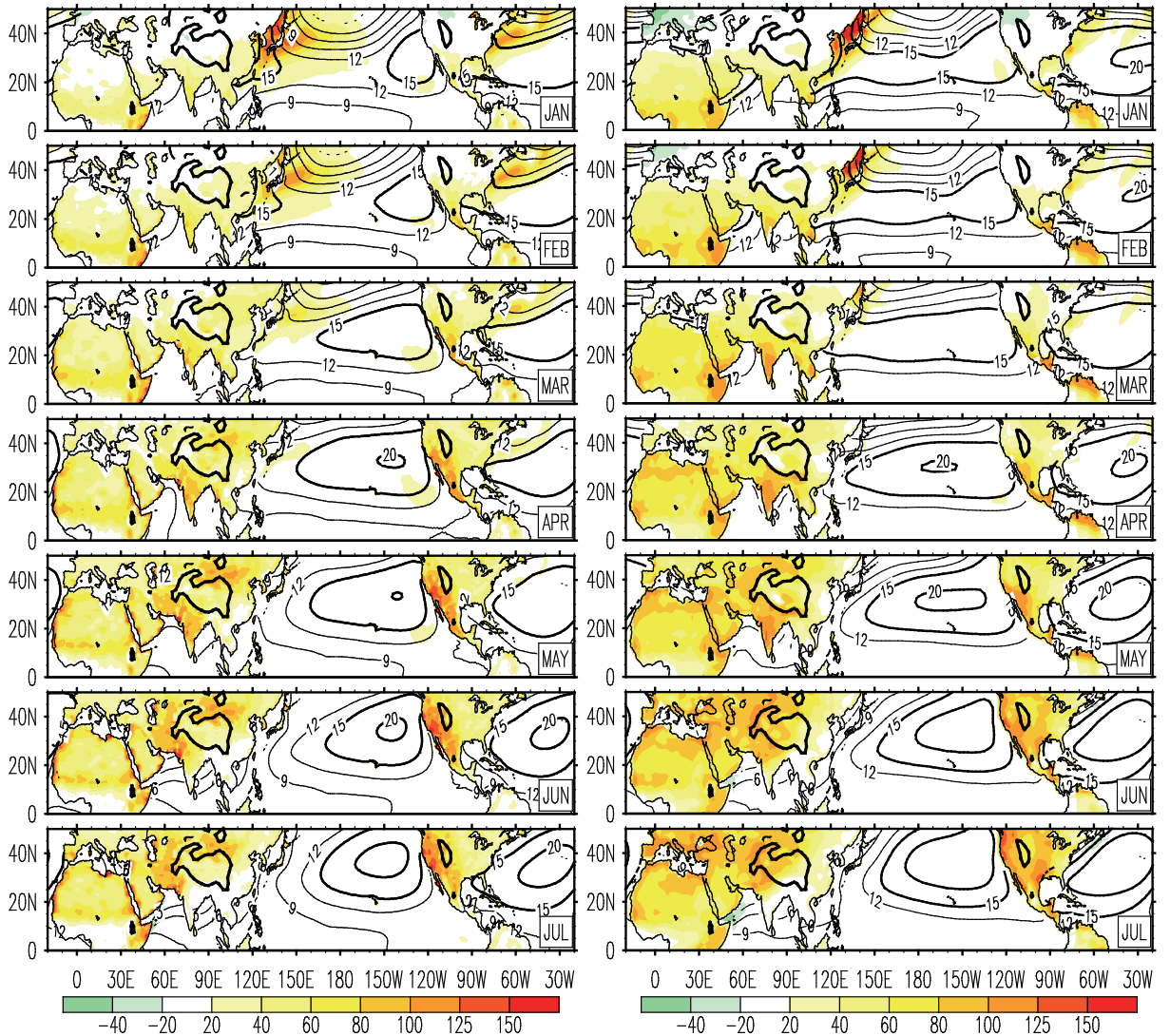


Fig. 6. Mean GPH (units: dgpm) at 1000 hPa and surface SE (units: W m^{-2}) from ERA-40 (left) and FGOALS-s2 (right). January to July is represented from top to bottom. The thick contours denote the GPH of 15 and 20 dgpm, respectively.

ticyclones. The SAEP and SAEA are stronger in the simulation than in the observation in both the spring and summer, and their centers are shifted westwards compared to ERA-40.

These biases can also be clearly detected in the differences of the zonal GPH deviations between the simulation and reanalysis (right panels of Fig. 5). Over the subtropics, GPH simulation is overestimated over the western but underestimated over the eastern subtropical Pacific in wintertime. In summer (June and July in the right panels of Fig. 5), the SAEP and SAEA simulations are overestimated. Accordingly, simulation of the lows over the Eurasian and North America continents are overestimated too, as presented by the negative difference in the right panels of Fig. 5.

4. Mechanism of SA seasonal development and the main biases in SA simulation by FGOALS-s2

4.1 SAs in the middle and upper troposphere

Charney and Shukla (1981) observed that tropical weather systems are determined by circulations between long-term heat sources and sinks. Saha (2010) proposed that tropical circulation systems are basically forced by boundary layer heat sources and sinks, on different time and spatial scales. To investigate the impacts of thermodynamics on the simulation of SA seasonal development, the differences of 200-hPa GPH and mean temperature from the surface to 200

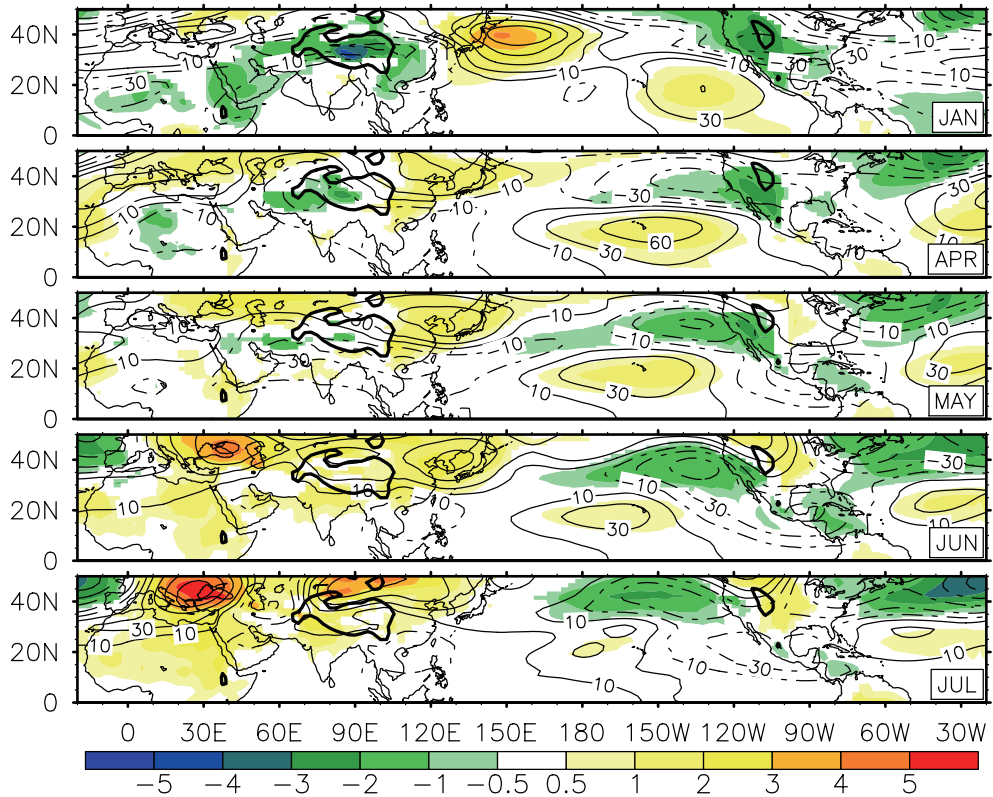


Fig. 7. Differences between FGOALS-s2 and ERA-40 in zonal deviation of GPH at 200 hPa (contours; units: gpm) and temperature vertically integrated from 1000 hPa to 200 hPa (shaded; units: K). January and April to July are represented from top to bottom. Shading of greater than 1 or less than -1 are the areas where temperature differences are statistically significant at the 99% level according to the Student's *t*-test.

hPa between the simulation and reanalysis were diagnosed.

As demonstrated in Fig. 7, almost all the major 200-hPa GPH biases correspond to significant temperature differences. In January, a warm bias is located over the northwestern Pacific, producing a positive GPH deviation there and a weaker EAT in FGOALS-s2. Over large mountains, the TP and Rocky Mountains, there are cold biases corresponding to the lower GPH deviation in the troposphere (January in Fig. 7). Although the positive GPH difference is not apparent in the tropics, the wind difference shows (January in right panels of Fig. 3) that there exists an anticyclone over India, meaning the GPH and wind differences over East Asia are presented as a Rossby wave train emanating from India to the northwestern Pacific.

This wave train could be triggered by the diabatic heating difference between the simulation and reanalysis. By comparing the differences between total heating (Q) and CO heating, it is shown that the total simulated heating errors (data not shown) in the tropics and also in the mid-high latitudes over the oceans are mainly induced by the CO in either win-

ter or spring and summer. In January, there exists overestimated CO over the Arabian Sea, and underestimated heating over the eastern BOB and tropical Pacific (left panels of Fig. 9). Since these two heating centers are located in the northern tropics close to the equator, according to Gill (1980) such an asymmetric thermal forcing can generate a Rossby-wave upper-tropospheric response. As demonstrated in the upper-left panel of Fig. 9, the strong negative condensation heating bias of lower than -150 W m^{-2} over the Andaman Sea in the southeastern BOB produces a significant difference in anticyclonic circulation to its northwest over India and the northwest BOB; whereas, the strong positive condensation heating bias of greater than 90 W m^{-2} over the tropical Arabian Sea produces a significant cyclonic circulation to its northwest over the Arabian Peninsula. Such a thermal-induced cyclone/anticyclone pair can also be identified at the 200-hPa level, as presented in the upper-right panel of Fig. 3. However, the deviated cyclonic circulation over the Arabian Peninsula at 200 hPa gets damped probably because the background stationary-wave circulation there is anticyclonic (upper-left panel of Fig. 3).

As a consequence, only left over tropical Asia is an amplified and remarkable anticyclone circulation centered over India (upper-right panel of Fig. 3). In January, westerlies prevail over subtropical Asia at 200 hPa (upper panel of Fig. 1), and the thermal-induced anticyclone circulation over India thus propagates northeastward, presenting a Rossby-wave train. During its course of northward propagation, its amplitude gets enhanced owing to the increasing latitude along its path. Eventually, a remarkable anticyclone circulation bias with a GPH increase of greater than 120 gpm appears over the northern Pacific (upper-right panel of Fig. 3). From this point of view, the weaker EAT in winter modeled by FGOALS-s2 is at least partly due to the weaker condensation heating over the southeastern BOB (upper-left panel of Fig. 9). It is interesting to see that the northerly/southerly on the east/west of the different anticyclone over the northwestern Pacific is well coordinated with decreased/increased convective heating. Considering the strong baroclinity in this region in winter, the above results indicate the significance of the cold and dry/warm and moist advection on the enhanced/suppressed convective activities in winter.

Another warm bias in January exists over the eastern tropical Pacific (January in Fig. 7 and left panels of Fig. 9). The heat source is much closer to the equator where the Coriolis effect of the Earth's rotation is diminished. Thus, there is a positive GPH bias above the heating. Such warming shifts to the central Pacific and persists until spring, April and May, and results in an anticyclone bias over the central Pacific compared to ERA-40. During the summer months of June and July, warm biases appear over mid-high latitudes over the continents (Fig. 7). Those warm biases over Eur-

sia contribute to the northward shift of the SAA center in the model compared to ERA-40 (Figs. 1 and 2).

The tracks of the SAA center and diabatic heating (Fig. 8) further show that SAA seasonal development is closely related to the seasonal variation of total heating. In April in the ERA-40 observation, total heating starts increasing to the south of South Asia. The heating is about 70 W m^{-2} in March, but 70 W m^{-2} in April over South Asia and the western Pacific (left panels of Fig. 1 and Fig. 8a). Correspondingly, the SAA is established near 110°E , which is consistent with previous studies (Qian et al., 2002; Liu et al., 2009). Meanwhile, from modeling results, the total heating above the SCS area increases from March to April, but is still negative (Fig. 8b). Thus, although the GPH over the SCS increases (right panels of Fig. 1), the increase is not large enough and the GPH is lower than that near the central Pacific (right panels of Fig. 1). Therefore, the simulated SAA is very weak near the SCS and the center of the high pressure is located near the central Pacific, as presented in Fig. 8.

In subtropical summer, CO dominates the eastern continent (Liu et al., 2004b; Wu et al., 2009). Figures 1 and 4 clearly show that the domination of CO starts from April, by comparing both ERA-40 and simulation results. However, in April, modeled CO is weaker than that in ERA-40, and surface sensible heating is overestimated in southeastern Asia (right panels of Fig. 9). Thus, the lower total heating in the simulation in April is mainly due to the weaker simulated levels of condensation. Comparing Fig. 8c to Fig. 8b, we can see that the deviation of total heating to the east of the date line is also due to the CO bias. Therefore, we can conclude that, in spring, CO contributes to the es-

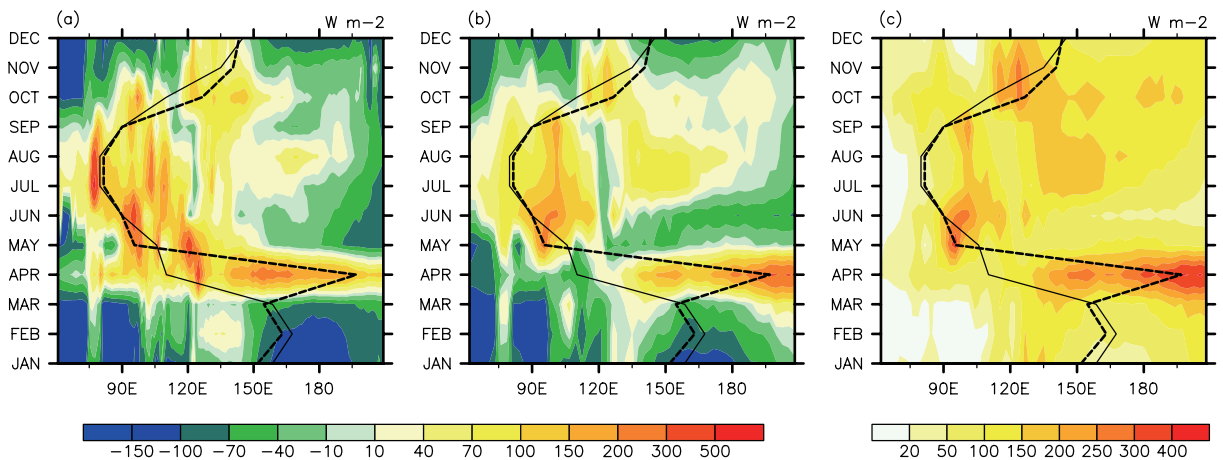


Fig. 8. The time–longitude tracks of the SAA centers (contours; defined in the same way as in Fig. 2) and column diabatic heating (shaded; units: W m^{-2}) along the same latitude where the SAA center is located. (a) Total heating from ERA-40; and (b) total heating and (c) CO from FGOALS-s2. Solid contour: ERA-40; dashed contour: FGOALS-s2.

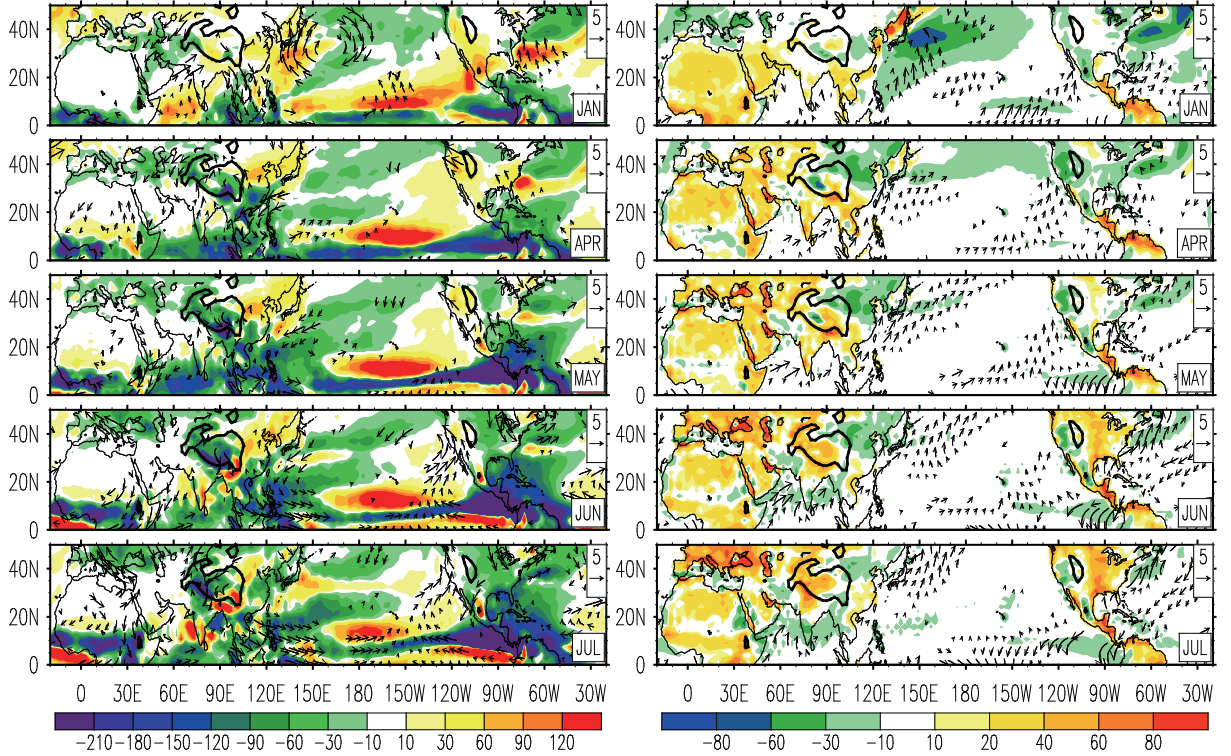


Fig. 9. Differences between FGOALS-s2 and ERA-40 in zonal deviation of wind (vector; units: m s^{-1}) at 500 hPa (left) and 1000 hPa (right). The shading denotes column CO (left) and surface SE (right) (units: W m^{-2}). January and April to July are represented from top to bottom. Only wind differences that are statistically significant at the 99% level according to the Student's *t*-test are shown.

establishment of the SAA and simulated CO deviation plays a dominant role in the simulated deviation of SAA seasonal development.

CO is underestimated over most of the TP and southern Asia not only in spring but also in summer, especially in later spring and early summer, i.e. in May and June (left panels of Fig. 9). Along the weak zonal flow, the atmospheric adaptation to external heating is manifested as the following Sverdrup vorticity balance (Wu and Liu, 2000; Liu et al., 2001):

$$\beta v \approx \frac{(f + \zeta)}{\theta_z} \frac{\partial Q}{\partial z}. \quad (1)$$

Where β is the variation of Coriolis parameter (f) with latitude, v the meridional wind, ζ the vertical component of vorticity, θ_z the vertical changes in potential temperature, Q the diabatic heating. Therefore, the underestimated CO in the TP–East-Asia area can result in southerlies in the upper troposphere and northerlies in the lower troposphere. Such wind deviation is significant in the western Pacific in June, i.e. southerlies at 200 hPa (right panel of Fig. 3) and northerlies at 500 hPa (right panel of Fig. 9), since the maximum CO is between 400 and 500 hPa in the FGOALS-s2 summer monsoon region.

It is interesting to note that, in the Atmospheric Model Intercomparison Project (AMIP) integration, the CO over the western Pacific is overestimated (data not shown; refer to Wang et al., 2012); thus, the 500-hPa SAWP is stronger in the AMIP run than in the coupled experiment. As shown in Bao et al. (2012), there is a cold bias of the SST in the warm pool domain in the FGOALS-s2 simulation, the same as in its earlier version (Wang et al., 2007). Therefore, the atmosphere responds too strongly to the warm SST in the AMIP run and the negative feedback between the precipitation and the SST in the coupled experiment is also too strong. Consequently, the FGOALS simulation presents a weaker bias in both the SST and heating in the atmosphere over the warm pool area.

4.2 SAs near the surface

The bias from the reanalysis of the simulated zonal deviation circulation near the surface is opposite to that in the middle and upper troposphere. The simulated surface SA SAEA is stronger than in ERA-40 from spring to summer, while the positive deviation of the SAEP mainly appears in summer (right panels of Fig. 5b). This is because the simulated surface SE (Fig. 9b) presents a warm bias from winter to summer

on most of the African–European continents, but only in summer on the North America continent. According to the PV- θ view (Hoskins, 1991) and the theory of thermal adaptation (Wu and Liu, 2000), the atmosphere is expected to respond to continental heating by the generation of cyclonic circulation in the lower troposphere and anticyclonic circulation over the ocean (Liu et al., 2001, 2004b; Wu et al., 2009). However, lower surface pressure biases do exist over the African–Eurasian continent during spring and summer, while only in summer over North America (right panels of Fig. 5) when the SE is overestimated on the continents (right panels of Fig. 9). Correspondingly, stronger southerly winds over East Asia and the western Pacific and in eastern America and the western Atlantic, as well as stronger northerly winds over the west American and west African coasts, exist in the simulation, meaning that the surface SAs over the oceans are stronger in summer than in ERA-40 (right panels of Fig. 5). In addition, the westward shift in the locations of the two surface anticyclone centers is the result of the underestimated simulation of the long-wave radiation cooling over the eastern oceans (Fig. 1). Wu et al. (2003) and Liu et al. (2004b) have indicated that LO cooling over the eastern oceans can generate negative vorticity near the surface and results in the asymmetric configuration of the surface SAs, with their centers shifted eastwards. In FGOALS-s2 and its earlier version (Wu et al., 2003), the cloud scheme is a diagnostic method based on vertical motion and relative humidity (Liu and Wu, 1997). The stratus cloud is underestimated globally compared to the tropical rainfall measuring mission (TRMM) data, especially over the eastern oceans in the lower troposphere (Wang et al., 2011), resulting in weaker LO near the top of the stratus cloud. For example, the modeled LO is 50 W m^{-2} less over the eastern Pacific during spring and summer. This weaker LO then leads to the westward shifting of the centers of the SAEP and SAEA in FGOALS-s2.

The exception is in winter. Although there is a warm SE bias in January over the African–Eurasian continent (upper-right panel of Fig. 9), there is a positive GPH bias at 1000 hPa (right panels of Fig. 5) and the GPH presents a quasi-barotropic anticyclonic circulation from surface to the upper troposphere from 20° – 40°N (right panels of Figs. 3 and 5). This may be due to the cooling bias of the column air temperature over this region (January in Fig. 7).

5. Summary and discussion

The general simulation characteristics of the seasonal evolution of SAs in the Northern Hemisphere and their biases were documented for the climate model

FGOALS-s2 in this study. Comparisons with ERA-40 and JRA-25 reanalysis data were made to explore the reasons responsible for the biases and to understand the control mechanism of the seasonal development of SAs.

In general, the CO over the Asian Monsoon area in summer contributes to the establishment of the SAA in spring and the strengthening of the SAA and the SAWP in summer. The CO simulation deviation plays a dominant role in the simulation deviation of SAA seasonal development. The SE in the mid-high latitudes of Eurasia also contributes to the configuration of the SAA in summer.

Many aspects of the SAs, the SAA in the upper troposphere, the SAWP in the middle troposphere, and the SAEP and SAEA near the surface are simulated reasonably well in winter and summer. The main bias of the simulated SAA appears during its generation stage in spring. The deviations of the GPH from the reanalysis are consistent with the bias of temperature in the troposphere. In ERA-40, an anticyclone circulation develops in spring over the SCS owing to the remarkable increase in precipitation and the associated CO over South Asia and the Indochina Peninsula. While in the simulation, there is a persistently overestimated CO bias over the central and eastern tropical Pacific from winter to summer, and an underestimated CO bias over the SCS and western Pacific from spring to summer. Such biases generate an anticyclonic gyre in the upper troposphere above the middle Pacific and delay the generation of the SAA over South Asia in April. The weaker CO over the East-Asia–West-Pacific region in spring and summer also contributes to the weaker SAA and SAWP in the model in spring and early summer. In mid-summer, the simulated SAA is located farther north than in ERA-40 owing to the excessively strong surface SE to the north of the TP.

For the two modeled near-surface SAs, the SAWP and the SAEA, their intensity is stronger in summer, with the SAEA becoming stronger from spring, and their centers are located westwards compared to in the ERA-40 reanalysis. The former is due to the stronger surface SE bias over the two continents in the Northern Hemisphere, which generates stronger cyclonic circulation over land and anticyclone circulations over oceans; whereas the latter is mainly due to the weaker long-wave radiation cooling bias over the eastern oceans associated with much less simulated local stratiform clouds.

The results obtained from this study demonstrate that, to simulate the seasonal evolution of SAs better in the climate model FGOALS-s2, the stratiform cloud scheme, the skills of the convection processes

and land-air energy exchange, need to be improved. Furthermore, the weaker modeled CO over the eastern Asia and western Pacific area is associated with its cold bias of the SST in the warm pool region. Further efforts on air-sea interaction simulation are also necessary.

Acknowledgements. This work was jointly supported by the National Natural Science Foundation of China (Grant No. 40925015), the CAS Strategic Priority Research Program (Grant No. XDA01020303), and the National Program on Key Basic Research Project (Grant No. 2010CB950400).

REFERENCES

- Bao, Q., and Coauthors, 2013: The flexible global ocean-atmosphere-land system model, spectral version 2: FGOALS-s2. *Adv. Atmos. Sci.*, doi: 10.1007/s00376-012-2113-9.
- Charney, J. G., and A. Eliassen, 1949: A numerical method for predicting the perturbations of the middle latitude westerlies. *Tellus*, **1**, 38–54.
- Charney, J. G., and J. Shukla, 1981: Predictability of Monsoons. *Monsoon Dynamics*, J. Lighthill and R. P. Pearce, Eds., Cambridge University Press, Cambridge, 99–109.
- Collins, W. D., and Coauthors, 2006: The community climate system model, version 3 (CCSM3). *J. Climate*, **19**, 2122–2143.
- Duan, A. M., G. X. Wu, and X. Y. Liang, 2008: Influence of the Tibetan Plateau on the summer climate patterns over East Asia in the IAP/LASG SAMIL model. *Adv. Atmos. Sci.*, **25**, 518–528, doi: 10.1007/s00376-008-0518-2.
- Gill, A. 1980: Some simple solutions for heat-induced tropical circulation. *Quart. J. Roy. Meteor. Soc.*, **106**(449), 447–462.
- Hoskins, B. J., 1987: Diagnosis of forced and free variability in the atmosphere. *Atmospheric and Oceanic Variability*, H. Cattle, Ed., James Glaisher House, Bracknell, 57–73.
- Hoskins, B. J., 1991: Towards a PV- θ view of the general circulation. *Tellus A*, **43**, 27–35.
- Li, J., 2001: *Atlas of Climate of Global Atmospheric Circulation I. Climatological Mean State*. China Meteorological Press, Beijing, 279pp. (in Chinese)
- Liu, B. Q., J. H. He , and L. J. Wang, 2009: Characteristics of the South Asia High establishment processes above the Indo-China Peninsula from April to May and their possible mechanism. *Chinese J. Atmos. Sci.*, **33**(6), 1319–1332. (in Chinese)
- Liu, H., and G. X. Wu, 1997: Impacts of land surface on climate of July and onset of summer monsoon: A study with an AGCM plus SSIB. *Adv. Atmos. Sci.*, **14**, 289–308.
- Liu, H. L., X. H. Zhang, W. Li, Y. Q. Yu, and R. C. Yu, 2004a: An eddy-permitting oceanic general circulation model and its preliminary evaluations. *Adv. Atmos. Sci.*, **21**, 675–690.
- Liu, H. L., P. F. Lin, Y. Q. Yu, and X. H. Zhang, 2012: The baseline evaluation of LASG/IAP climate system ocean model (LICOM) version 2.0. *Acta Meteorologica Sinica*, **26**(3), 318–329.
- Liu, Y. M., G. X. Wu, H. Liu, and P. Liu, 1999: Spatially inhomogeneous diabatic heating and its impacts on the formation and variation of subtropical anticyclone, III. Convective condensation heating and the subtropical anticyclone over South Asia and Northwest Pacific. *Acta Meteorologica Sinica*, **57**(5), 525–538.
- Liu, Y. M., G. X. Wu, H. Liu, and P. Liu, 2001: Dynamical effects of condensation heating on the subtropical anticyclones in the Eastern Hemisphere. *Climate Dyn.*, **17**, 327–338.
- Liu, Y. M. G. X. Wu, and R. C. Ren, 2004b: Relationship between the subtropical anticyclone and diabatic heating. *J. Climate*, **17**, 682–698.
- Liu, Y. M., B. J. Hoskins, and M. Blackburn, 2007: Impact of Tibetan orography and heating on the summer flow over Asia. *J. Meteor. Soc. Japan*, **85B**, 1–19.
- Newell, R. E., D. G. Vincent, T. G. Dopplick, D. Ferruza, and J. W. Kidson, 1970: The energy balance of the global atmosphere. *The Global Circulation of the Atmosphere*, G. A. Corby, Eds., Royal Meteorological Society, London, 42–90.
- Onogi, K., and Coauthors, 2007: JRA-25: Japanese 25-year re-analysis. *Quart. J. Roy. Meteor. Soc.*, **131**, 3259–3268.
- Qian, Y., Q. Zhang, Y. Yao, and X. Zhang, 2002: Seasonal variation and heat preference of the South Asia High. *Adv. Atmos. Sci.*, **19**(5), 821–836.
- Rodwell, M. J., and B. J. Hoskins, 2001: Subtropical anticyclones and monsoons. *J. Climate*, **14**, 3192–3211.
- Saha, K., 2010: *Tropical Circulation Systems and Monsoons*. Springer-Verlag, 324pp.
- Uppala, S. M., and Coauthors, 2005: The ERA-40 reanalysis. *Quart. J. Roy. Meteor. Soc.*, **131**, 2961–3012.
- Wang, J., Y. M. Liu, G. X. Wu, Q. Bao, B. He, and X. Wang, 2012: Performances of SAMIL (AGCM) on the global heating and the East Asian summer monsoon. *Chinese J. Atmos. Sci.*, **36**(1), 63–76. (in Chinese)
- Wang, X. C., Q. Bao, K. Liu, G. X. Wu, and Y. M. Liu, 2011: Features of rainfall and latent heating structure simulated by two convective parameterization schemes. *Sci. China (Earth)*, **54**(11), 1779–1788.
- Wang, Z. Z., R. C. Yu, Q. Bao, T. J. Zhou, G. X. Wu, Y. M. Liu, and P. F. Wang, 2007: A comparison of the atmospheric circulations simulated by the FGOALS-s and SAMIL. *Chinese J. Atmos. Sci.*, **32**, 1–12. (in Chinese)
- Wu, G., and Y. Liu, 2000: Thermal adaptation, overshooting, dispersion and subtropical anticyclone, I: Thermal adaptation and overshooting. *Chinese J. Atmos. Sci.*, **24**, 433–446. (in Chinese)

- Wu, G., and Y. Liu, 2003: Summertime quadruplet heating pattern in the subtropics and the associated atmospheric circulation. *Geophys. Res. Lett.*, **30**, 1201, doi: 10.1029/2002GL016209.
- Wu, G. X., J. F. Chou, Y. M. Liu, and J. H. He, 2002: *Dynamics of the Formation and Variation of Subtropical Anticyclones*. Science Press, Beijing, 314pp. (in Chinese)
- Wu, G., and Coauthors, 2007: The influence of the mechanical and thermal forcing of the Tibetan Plateau on the Asian climate. *J. Hydrometeorology*, **8**(4), 770–789.
- Wu, G., Y. Liu, X. Zhu, W. Li, R. Ren, A. Duan, and X. Liang, 2009: Multi-scale forcing and the formation of subtropical desert and monsoon. *Ann. Geophys.*, **27**(9), 3631–3644.
- Wu, T., P. Liu, Z. Wang, Y. Liu, R. Yu, and G. Wu, 2003: The performance of atmospheric component model (R42L9) of GOALS/LASG. *Adv. Atmos. Sci.*, **20**(5), 726–742.
- Yeh, T. C., 1950: The circulation of the high troposphere over China in the winter of 1945–1946. *Tellus*, **2**, 173–183.
- Yu, J. J., Y. M. Liu, and G. X. Wu, 2011: An analysis of the diabatic heating characteristic of atmosphere over the Tibetan Plateau in winter I: Climatology. *Acta Meteorologica Sinica*, **69**(1), 79–88.